

## Direct Trajectory Optimization of Free-Floating Space Manipulator for Reducing Spacecraft Variation

Shao, Xiangyu; Yao, Weiran; Li, Xiaolei; Sun, Guanghui; Wu, Ligang

**DOI**

[10.1109/LRA.2022.3143586](https://doi.org/10.1109/LRA.2022.3143586)

**Publication date**

2022

**Document Version**

Final published version

**Published in**

IEEE Robotics and Automation Letters

**Citation (APA)**

Shao, X., Yao, W., Li, X., Sun, G., & Wu, L. (2022). Direct Trajectory Optimization of Free-Floating Space Manipulator for Reducing Spacecraft Variation. *IEEE Robotics and Automation Letters*, 7(2), 2795-2802. <https://doi.org/10.1109/LRA.2022.3143586>

**Important note**

To cite this publication, please use the final published version (if applicable). Please check the document version above.

**Copyright**

Other than for strictly personal use, it is not permitted to download, forward or distribute the text or part of it, without the consent of the author(s) and/or copyright holder(s), unless the work is under an open content license such as Creative Commons.

**Takedown policy**

Please contact us and provide details if you believe this document breaches copyrights. We will remove access to the work immediately and investigate your claim.






***Green Open Access added to TU Delft Institutional Repository***

***'You share, we take care!' - Taverne project***

**<https://www.openaccess.nl/en/you-share-we-take-care>**

Otherwise as indicated in the copyright section: the publisher is the copyright holder of this work and the author uses the Dutch legislation to make this work public.

# Direct Trajectory Optimization of Free-Floating Space Manipulator for Reducing Spacecraft Variation

Xiangyu Shao , *Student Member, IEEE*, Weiran Yao , *Member, IEEE*,  
Xiaolei Li , *Graduate Student Member, IEEE*, Guanghui Sun , *Senior Member, IEEE*,  
and Ligang Wu , *Fellow, IEEE*

**Abstract**—This letter investigates the direct trajectory optimization of the free-floating space manipulator (FFSM). The main purpose is to plan the joint space trajectories to reduce the spacecraft motion due to the joint rotation during the FFSM performing tasks. To improve the calculation efficiency, the adaptive Radau pseudospectral method (A-RPM) is applied to discretize the system dynamics and transform the formulated optimal problem into a nonlinear programming problem (NLP). By adaptively subdividing the current segment and assigning collocation points according to the solution error, high-degree interpolation polynomials are avoided. To verify the effectiveness of the proposed method, a ground micro-gravity platform of the FFSM system is designed by using the air-bearing technique, on which experiments are carried out. The results show that the variation of the base spacecraft is dramatically reduced if the joints rotate along the optimized trajectories.

**Index Terms**—Direct trajectory optimization, free-floating space manipulator, radau pseudospectral method, spacecraft variation reduction.

## I. INTRODUCTION

THE space manipulator plays an important role in various space operations [1], e.g., space station maintenance, space debris removal, on-orbit assembly. Considering the situation of completely turning off the system actuators, the spacecraft can move in response to the rotation of joints, resulting in the concept of free-floating space manipulator (FFSM). As a special working mode, the FFSM has obvious advantages in saving fuel,

extending on-orbit service time, and it can also avoid collisions when the spacecraft is close to other space vehicles. However, the property that the spacecraft can move freely also means that it is uncontrollable, and may lead to some unexpected situation.

In the past decades, a great deal of research has been focused on the modeling, design, and control of the FFSM system. In the 1990 s, Papadopoulos *et al.* established the kinematics and dynamics of the FFSM and pointed out the applicability of the fixed-based control algorithms for the FFSM [2]. Afterward, many control methods were reported to deal with the dynamic coupling between the spacecraft and the mounted manipulator, and reduce the spacecraft variation. As a promising branch of control theory, the application of optimal control in the space manipulator has aroused wide concern. Misra *et al.* investigated an optimal control problem for a free-flying space manipulator and achieved end-effector positioning [3]. Lu *et al.* investigated the trajectory planning problem of the FFSM at the acceleration level and formulated the planning problem as a convex quadratic programming problem [4].

The above mentioned studies once promoted the development of the FFSM, but there are still some unresolved issues. First, many works for reducing the base variation only consider the base rotation, but the manipulator motion also leads to base translation. Besides, even in the case of ignoring the base translation, it is still insufficient to consider only the integral of base angular velocity in the cost functional (e.g., [4], [5]). The smoothness of the manipulator movement and the difference between the final and initial base attitude should also be considered. Second, some works still use the indirect method to solve the optimal problem. In many cases, the indirect method yields very accurate solutions, but it has obvious disadvantages, including small convergence radius, difficulty in analytically deriving the necessary optimality conditions, slow calculation efficiency [6]. Finally, due to the special working environment of the FFSM, experiments for verifying effectiveness of the proposed optimal method in reducing base variation are still insufficient in existing works.

In this letter, we propose a method to reduce the influence of the joint rotation on the base spacecraft from the perspective of optimal control, and its effectiveness is verified on a micro-gravity manipulator platform. To improve the calculation efficiency, the adaptive Radau pseudospectral method (A-RPM) is applied when solving the formulated optimal control problem. With regard to reducing the disturbance on the base, a similar

Manuscript received November 5, 2021; accepted January 3, 2022. Date of publication January 18, 2022; date of current version February 2, 2022. This letter was recommended for publication by Associate Editor J. Cacace and Editor P. Pounds upon evaluation of the reviewers' comments. This work was supported in part by the National Key R&D Program of China under Grant 2019YFB1312000, in part by the National Natural Science Foundation of China under Grants 62106062, 62033005, and 62173107, in part by the Heilongjiang Provincial Natural Science Foundation of China under Grant YQ2021F010, and in part by the China Postdoctoral Science Foundation under Grant 2020M681098. (*Corresponding author: Weiran Yao.*)

Xiangyu Shao is with the School of Astronautics, Harbin Institute of Technology, Harbin 150001, China, and also with the Cognitive Robotics Department, Delft University of Technology, Delft 2628 CD, Netherlands (e-mail: xiangyushao@hit.edu.cn).

Weiran Yao, Xiaolei Li, Guanghui Sun, and Ligang Wu are with the School of Astronautics, Harbin Institute of Technology, Harbin 150001, China (e-mail: yaoweiran@hit.edu.cn; xiaoleili@hit.edu.cn; guanghuisun@hit.edu.cn; ligangwu@hit.edu.cn).

This letter has supplementary downloadable material available at <https://doi.org/10.1109/LRA.2022.3143586>, provided by the authors.

Digital Object Identifier 10.1109/LRA.2022.3143586

approach was also proposed by Schulz [7]. Compared with Schulz's work, this letter considers both the base translation and the base rotation. Besides, the final displacement and rotation of the base, the states of mounted manipulator are also included in the cost functional, which not only prevents the final base posture from deviating too far from its initial value, but also takes the smoothness of the joint trajectories into consideration. Another approach to tackle this problem is the reaction null-space control proposed by Nechev [8]. However, the existence of reaction null-space is conditional, e.g., kinematic and dynamic redundancy, rank deficiency of the inertia coupling matrix. This means one may not be able to find the reaction null-space solution in some cases. Besides, we note that task space planning is usually expected in many space operations. However, there are also many cases such as the precapture phase, where the manipulator is expected to have a certain precapture configuration while the precise task space positioning is unnecessary. Reducing the base variation during this phase is meaningful for subsequent operations and the joint space planning is still practical.

Regarding the A-RPM, it discretizes the dynamics at the Legendre-Gauss-Radau (LGR) points and transcribes the optimal control problem into a nonlinear programming problem (NLP) [9]. The traditional RPM uses a global polynomial for approximation and the solution accuracy is improved by increasing the degree of this polynomial, which will result in expensive computation [10]. The A-RPM can adaptively subdivide the current segment and assign collocation points if the tolerance is not satisfied rather than only increasing the polynomial degree, avoiding high-degree polynomials. To verify effectiveness of the proposed optimal method in reducing the base variation, we design a micro-gravity experiment platform by using the air-bearing technique. Similar experiment platforms were also presented by Aghili and Lampariello [1], [11], which can effectively simulate the working condition of a monolithic space system. Whereas, the platforms in their works ignored the manipulator gravity rather than compensate it. This makes the working condition of manipulators of their platforms quite different from that of a practical FFSM. Besides, the disturbance on the spacecraft generated by joint rotation cannot be well simulated because the spacecraft in these platforms is supported by an extra manipulator instead of in a free-floating mode. Until now, the experiments for verifying the effectiveness of the optimal method in base variation reducing are still limited.

The rest of this letter is organized as follows. The system dynamics and the optimal problem formulation are given in Section II. The A-RPM for solving the established problem is presented in Section III. Simulation and experiment results are analyzed in Section IV and we conclude this letter in Section V.

## II. PROBLEM FORMULATION

### A. Dynamics of Free-Floating Space Manipulator

For an FFSM system with a movable base spacecraft and an  $N$  revolute joints manipulator mounted on it, the position vector of each body with respect to the system's center of mass (CM)

is given by

$$\rho_k = \sum_{i=0}^N v_{ik} \quad k = 0, \dots, N \quad (1)$$

where  $v_{ik}$  is the barycenter vector defined in [12]. The angular and linear velocities of body  $k$  are calculated by

$$\begin{aligned} \omega_k &= T_0^0 \omega_0 + T_0^0 F_k \dot{\theta}_m \\ \dot{\rho}_k &= -T_0^0 \sum_{i=0}^N \left\{ ({}^0T_i v_{ik})^\times \omega_0 + ({}^0T_i v_{ik})^\times F_i \dot{\theta}_m \right\} \end{aligned} \quad (2)$$

in which  ${}^jT_i \in \mathbb{R}^{3 \times 3}$  is the rotation matrix of  $i$ th frame with respect to  $j$ th frame;  $\omega_0$  is the angular velocity of the base spacecraft;  $\theta_m = [\theta_{m1}, \theta_{m2}, \dots, \theta_{mn}]^T$  denotes the joint angles;  ${}^0F_k = [{}^0T_1^1 u_1, \dots, {}^0T_k^k u_k, 0_{3 \times N-k}] \in \mathbb{R}^{3 \times N}$  with  ${}^i u_i$  being the unit rotation vector of frame  $i$ . The kinetic energy  $T$  can be obtained by

$$T = \frac{1}{2} \sum_{k=0}^N (\omega_k^T I_k \omega_k + m_k \dot{\rho}_k^T \dot{\rho}_k) \quad (3)$$

where  $I_k$ ,  $m_k$  are the inertia dyadic and the mass of body  $k$ , respectively. Using the reduced Euler-Lagrange equation, the system dynamics can be formulated as

$$\begin{bmatrix} H_{bb} & H_{bm} \\ H_{bm}^T & H_{mm} \end{bmatrix} \begin{bmatrix} \ddot{\xi}_b \\ \ddot{\theta}_m \end{bmatrix} + \begin{bmatrix} C_{bb} & C_{bm} \\ C_{mb} & C_{mm} \end{bmatrix} \begin{bmatrix} \dot{\xi}_b \\ \dot{\theta}_m \end{bmatrix} = \begin{bmatrix} 0 \\ \tau_m \end{bmatrix} \quad (4)$$

where  $H_{bb}, C_{bb} \in \mathbb{R}^{6 \times 6}$  are the inertia and Coriolis matrices of the base spacecraft.  $H_{mm}, C_{mm} \in \mathbb{R}^{n \times n}$  represent the inertia and Coriolis terms of the manipulator, respectively.  $H_{bm}, C_{bm} \in \mathbb{R}^{6 \times n}$  are the base-manipulator coupling matrices.  $\xi_b = [\zeta_b, \eta_b]^T \in \mathbb{R}^6$  represents the position and orientation of the spacecraft, in which  $\zeta_b = [x_b, y_b, z_b]^T$  is the position vector and  $\eta_b = [\phi_b, \psi_b, \theta_b]^T$  is the attitude vector.  $\tau_m \in \mathbb{R}^n$  denotes the torque applied on the joints. Considering the momentum conservation [13]

$$L = \tilde{J}_{bs} \dot{\xi}_b + \tilde{J}_{bm} \dot{\theta}_m = 0, \quad (5)$$

states of the spacecraft can be expressed by the joint variables  $\dot{\xi}_b = -\tilde{J}_{bs}^{-1} \tilde{J}_{bm} \dot{\theta}_m$ , and (4) can be further transformed into the following form

$$H(\theta_m) \ddot{\theta}_m + C(\theta_m, \dot{\theta}_m) \dot{\theta}_m = \tau_m \quad (6)$$

where  $H, C \in \mathbb{R}^{n \times n}$  are the inertia and Coriolis matrices of the system independent of states of the spacecraft.

*Properties 1:* [14] For any  $x \in \mathbb{R}^n$ , the inertia matrix  $H$  satisfies  $h_1 \|x\|^2 \leq x^T H x \leq h_2 \|x\|^2$ , where  $h_1, h_2$  are positive constants.

*Remark 1:* In the space environment, the effects of gravity and the gravity gradient are ignored. There are no external forces or torque acting on it when space manipulator working in the free-floating mode. Therefore, the FFSM satisfies the condition of momentum conservation. In this letter, we assume zero initial momentum such that the system CM remains fixed. The origin of the inertial frame is set at the system CM.

### B. Movement Constraints of Free-Floating Space Manipulator

To facilitate trajectory planning of the FFMSM system, write (6) in the form of state space, one has

$$\dot{x} = f(x, u, t) \quad (7)$$

where

$$f = \begin{bmatrix} 0 & I \\ 0 & -H^{-1}C \end{bmatrix} x + \begin{bmatrix} 0 \\ u \end{bmatrix},$$

$x = [\theta_m, \dot{\theta}_m]^T$ ,  $u = H^{-1}\tau_m$ ,  $I$  is the identity matrix. During the FFMSM performing tasks, several constrains should be satisfied.

1) *State Constraints*: In space operations, it is reasonable to assume that the configuration of the mounted manipulator is restricted. The constraints on the joint angles can be described as follows

$$\theta_{mi}(t) \in [\theta_{min}^i, \theta_{max}^i], \quad i = 1, \dots, N \quad (8)$$

where  $\theta_{min}^i$  and  $\theta_{max}^i$  are the lower and upper bounds of the  $i$ th joint, respectively. A practical space manipulator usually has a long arm, which will decrease the stiffness of the link. Too fast joint rotation may lead to unexpected deformation at the end of the link during the acceleration and deceleration phase. Besides, the system needs enough reaction time for potential emergencies. Therefore, limits on the joint angular velocity are given

$$\dot{\theta}_{mi}(t) \in [\dot{\theta}_{min}^i, \dot{\theta}_{max}^i] \quad (9)$$

where  $\dot{\theta}_{min}^i, \dot{\theta}_{max}^i$  are lower and upper bounds of the angular velocity of the  $i$ th joint. The spacecraft attitude and its angular velocity are also expected to satisfy

$$\eta_b(t) \in [\eta_{min}^b, \eta_{max}^b], \quad \dot{\eta}_b(t) \in [\dot{\eta}_{min}^b, \dot{\eta}_{max}^b] \quad (10)$$

where  $\eta_{min}^b, \eta_{max}^b, \dot{\eta}_{min}^b, \dot{\eta}_{max}^b$  are limits of the base rotation. As mentioned before, the origin of the inertial system is set at the system's center of mass. Once the joint states are determined, the position vector of the spacecraft can be directly obtained. Therefore, the limitation for spacecraft position is not included in the state constraints.

2) *Control Constraints*: For the FFMSM system, the spacecraft is under-actuated and there is no force or torque acting on it. Hence, the control constraints are only on the joints with  $\tau_{mi} \in [\tau_{min}^i, \tau_{max}^i]$ . Note that the inertia matrix  $H$  is positive definite and satisfies Properties 1,  $u$  is also bounded by

$$u_i(t) \in [u_{min}^i, u_{max}^i], \quad i = 1, \dots, N \quad (11)$$

3) *Boundary Constraints*: Let  $t_0$  denote the initial time, and  $t_f$  the final time. The initial and final constraints of the mounted manipulator are

$$\begin{aligned} \theta_m(t_0) &= [\theta_{m1}(t_0), \theta_{m2}(t_0), \dots, \theta_{mN}(t_0)]^T \\ \theta_m(t_f) &= [\theta_{m1}(t_f), \theta_{m2}(t_f), \dots, \theta_{mN}(t_f)]^T \end{aligned} \quad (12)$$

The initial and final angular velocities are usually zero

$$\dot{\theta}_m(t_0) = 0, \quad \dot{\theta}_m(t_f) = 0 \quad (13)$$

The basic goal is to find the joint trajectories from the initial configuration  $\theta_m(t_0), \dot{\theta}_m(t_0)$  to the final configuration  $\theta_m(t_f), \dot{\theta}_m(t_f)$ . Without loss of generality, the initial orientation of the spacecraft is assumed to be  $\eta_b(t_0) = 0, \dot{\eta}_b(t_0) = 0$ . Then, the initial position of the spacecraft is determined by  $\rho_0(t_0) = \sum_{i=0}^N v_{i0}$ . At the final time, the spacecraft should be stationary, i.e.,  $\dot{\eta}_b(t_f) = 0$ . In the free-floating mode, the spacecraft is under-actuated and the mass of spacecraft is usually much larger than that of the manipulator. The motion of spacecraft can not be well regulated only by the torque of joints. It is difficult to ensure that the base angle is consistent with its initial time or reaches a preset value at the final time. Therefore, we set the final attitude of the spacecraft as  $\eta_b(t_f) \in [\eta_{min}^b(t_f), \eta_{max}^b(t_f)]$  instead of a specific value.

### C. Objective of the Trajectory Optimization

Conventional path planning problems consider minimizing the operation time or the energy consumption. Whereas, there is usually no strict time requirement in most operations of the FFMSM system. Besides, the spacecraft turns off its propulsion device in the free-floating mode, which already has considerable advantages in terms of fuel saving. An important issue for the FFMSM system is to reduce the spacecraft variation introduced by the joint rotation. To achieve this goal, the cost functional  $J$  is designed in the following form

$$J = \Phi(\xi_b(t_0), \xi_b(t_f)) + \int_{t_0}^{t_f} \mathcal{L}(\xi_b(t), x(t), u(t), t) dt \quad (14)$$

where the terminal cost  $\Phi = \|\zeta_b(t_f) - \zeta_b(t_0)\|^2 + \|\eta_b(t_f)\|^2$  prevents the final base pose from deviating too far from its initial value, the integrated cost  $\mathcal{L} = [\dot{\eta}_b(t), \dot{\theta}_m]^T \Lambda [\dot{\eta}_b(t), \dot{\theta}_m]$  is used to ensure the motion smoothness of the spacecraft and the joints,  $\Lambda$  is the weight coefficient matrix denoting the weight of each term.

Then, the optimal control problem can be described as

$$\begin{aligned} \min \quad & J = \Phi(\xi_b(t_0), \xi_b(t_f)) + \int_{t_0}^{t_f} \mathcal{L}(\xi_b(t), x(t), u(t), t) dt \\ \text{s.t.} \quad & \begin{cases} \frac{dx}{dt} = f(x, u, t), \\ C[x(t), u(t), t] \leq 0 \\ E[x(t_0), t_0, x(t_f), t_f] = 0 \end{cases} \end{aligned} \quad (15)$$

in which  $C[x(t), u(t), t] \leq 0$  represents the path constraints (8)–(11),  $E[x(t_0), t_0, x(t_f), t_f] = 0$  denotes the boundary conditions (12)–(13). By using the following transformation

$$t = \frac{t_f - t_0}{2}\tau + \frac{t_f + t_0}{2}, \quad (16)$$

where  $\tau \in [-1, 1]$ , we obtain the standard Bolza optimal control formulation: Minimize the cost functional

$$\begin{aligned} J &= \Phi(\xi_b(-1), \xi_b(+1)) \\ &+ \frac{t_f - t_0}{2} \int_{-1}^1 \mathcal{L}(\xi_b(\tau), x(\tau), u(\tau), \tau) d\tau \end{aligned} \quad (17)$$

subject to

$$\begin{aligned} \frac{dx}{d\tau} &= \frac{t_f - t_0}{2} f(x, u, \tau; t_0, t_f), \\ C[x(\tau), u(\tau), \tau; t_0, t_f] &\leq 0, \\ E[x(-1), t_0, x(+1), t_f] &= 0 \end{aligned} \quad (18)$$

*Remark 2:* The cost functional (14) is a general form and its specific form for a two-link planar FFSM is given in the simulation section. The term  $\Phi(\xi_b(t_0), \xi_b(t_f))$  describes the base variation from the initial time to the final time, including the translation  $\|\zeta_b(t_f) - \zeta_b(t_0)\|$  and the rotation  $\|\eta_b(t_f)\|$ .  $\mathcal{L}(\xi_b(t), x(t), u(t), t)$  is designed to be related to the velocities of the base and the manipulator, which is benefit to the motion smoothness. It should be noted that a trade-off exists in the cost functional,  $\Lambda$  weighs the proportion of each term and the specific value of  $\Lambda$  depend on the optimal purpose and which aspect we focus more.

### III. ADAPTIVE RADAU PSEUDOSPECTRAL METHOD

In this section, the A-RPM is introduced and applied to solve the optimal problem. This method divides the entire time interval into several segments and allows for different degree polynomials in each segment. By allocating the LGR points in each segment instead of the entire interval, the maximum polynomial degree in each segment remains small with the user-defined tolerance being satisfied.

#### A. Segmentation of the Optimal Control Problem

The optimal control problem given in (17)–(18) is usually used in the global polynomial approximation. More nodes are needed to improve the solution accuracy, leading to high-degree interpolation polynomial and lower computational efficiency. To avoid this problem, divide the time interval  $t \in [t_0, t_f]$  into  $S$  segments  $[t_{s-1}, t_s]$ ,  $s = 1, \dots, S$ . Each segment  $t \in [t_{s-1}, t_s]$  is transformed into  $\tau \in [-1, +1]$  by using (16). Then, standard Bolza optimal problem of the  $s$ th segment can be written as follows

$$\begin{aligned} J &= \Phi\left(\xi_b^{(1)}(-1), t_0, \xi_b^{(S)}(+1), t_f\right) \\ &+ \sum_{s=1}^S \frac{t_s - t_{s-1}}{2} \int_{-1}^1 \mathcal{L}\left(\xi_b^{(s)}, x^{(s)}, u^{(s)}, \tau; t_{s-1}, t_s\right) d\tau \end{aligned} \quad (19)$$

subject to

$$\begin{aligned} \frac{dx^{(s)}}{d\tau} &= \frac{t_s - t_{s-1}}{2} f\left(x^{(s)}, u^{(s)}, \tau; t_{s-1}, t_s\right) \\ C\left[x^{(s)}, u^{(s)}, \tau; t_{s-1}, t_s\right] &\leq 0 \\ E\left[x^{(1)}(-1), t_0, x^{(S)}(+1), t_f\right] &= 0. \end{aligned} \quad (20)$$

#### B. Radau Pseudospectral Method

The RPM approximates the system dynamics at the LGR points, which lies on the half open interval  $\tau \in [-1, 1)$  or

$\tau \in (-1, 1]$ , and are the roots of  $P_{N-1}(\tau) + P_N(\tau)$ , with

$$P_N(\tau) = \frac{1}{2^N N!} \frac{d^N}{d\tau^N} \left[ (\tau^2 - 1)^N \right] \quad (21)$$

Here, the standard LGR points are used, which includes the initial endpoint  $-1$ . Suppose that there are  $N_s$  LGR points in the  $s$ th segment, denoted by  $(\tau_1^{(s)}, \dots, \tau_{N_s}^{(s)})$ . The system states  $x$  can be approximated using an interpolation polynomials

$$\begin{aligned} x^{(s)}(\tau) &\approx X^{(s)}(\tau) = \sum_{j=1}^{N_s+1} X_j^{(s)} L_j^{(s)}(\tau) \\ L_j^{(s)}(\tau) &= \prod_{\substack{l=1 \\ l \neq j}}^{N_s+1} \frac{\tau - \tau_l^{(s)}}{\tau_j - \tau_l^{(s)}}, \quad j = 1, \dots, N \end{aligned} \quad (22)$$

where  $\tau \in [-1, 1]$ ,  $L_j^{(s)}(\tau)$  is a basis of Lagrange polynomials. Note that  $\tau_{N_s+1} = 1$  is the endpoint of each segment instead of the LGR points. The derivative of  $X^{(s)}(\tau)$  with respect to  $\tau$  can be calculated by

$$\dot{X}^{(s)}(\tau) = \sum_{j=1}^{N_s+1} X_j^{(s)} \dot{L}_j^{(s)}(\tau) \quad (23)$$

and at the  $i$ th collocation point,  $\tau_i$ , we have

$$\dot{X}^{(s)}(\tau_i) = \sum_{j=1}^{N_s+1} X_j^{(s)} D_{ij}^{(s)} \quad (24)$$

where  $D_{ij}^{(s)} = \dot{L}_j^{(s)}(\tau_i)$  is the Radau differential matrix in segment  $s$ . The cost functional in segment  $s$  is then approximated as

$$\begin{aligned} J &\approx \Phi\left(\xi_{b,1}^{(1)}, t_0, \xi_{b,N_s+1}^{(S)}, t_f\right) \\ &+ \sum_{s=1}^S \sum_{j=1}^{N_s} \frac{t_s - t_{s-1}}{2} w_j^{(s)} \mathcal{L}\left(\xi_{b,j}^{(s)}, X_j^{(s)}, U_j^{(s)}, \tau_j^{(s)}; t_{s-1}, t_s\right) \end{aligned} \quad (25)$$

where  $\xi_{b,j}^{(s)}$ ,  $X_j^{(s)}$ , and  $U_j^{(s)}$ , ( $i = 1, \dots, N_s$ ) are the approximations at  $i$ th points,  $w_i^{(s)}$  is the barycentric weight. The system dynamics (7) is discretized as

$$\sum_{j=1}^{N_s+1} X_j^{(s)} D_{ij}^{(s)} - \frac{t_s - t_{s-1}}{2} f\left(X_i^{(s)}, U_i^{(s)}, \tau_i^{(s)}; t_{s-1}, t_s\right) = 0 \quad (26)$$

with the path and boundary constraints being

$$\begin{aligned} C\left[X_i^{(s)}, U_i^{(s)}, \tau_i; t_{s-1}, t_s\right] &\leq 0, \quad (i = 1, \dots, N_s) \\ E\left[X_1^{(1)}, t_0, X_{N_s+1}^{(S)}, t_f\right] &= 0 \end{aligned} \quad (27)$$

*Remark 3:* The RPM transcribes an optimal problem into the NLP, i.e., minimize (25) subject to (26)–(27). Besides, it is required that the state at the end of each segment should be equal to that at the start point of the next segment, i.e.,

$X^{(s)}(\tau_{N_s+1}) = X^{(s+1)}(\tau(1))$ . Hence, the continuity of the discretized states can be guaranteed by using the same NLP variable at  $\tau_{N_s+1}^{(s)}$  and  $\tau_1^{(s+1)}$ .

In the RPM, the continuous optimal problem is discretized and the discretization accuracy is improved by increasing the number of collocation points, which also increases the polynomial degree. For some smooth problems, it may be applicable, but the calculation efficiency will be dramatically reduced or result in unsatisfactory approximation for many non-smoothness problems [6]. Therefore,  $t \in [t_0, t_f]$  is divided into more segments and the optimal problem is discretized in each segment. After that, a global interpolation polynomial with high degree can be replaced by several polynomials with lower degree. In the following section, adaptive law for determining subdivision and LGR points of each segment will be presented.

### C. Adaptive Algorithm for Segment Division and Points Collocation

To evaluate the solution accuracy, a set of points in each segment,  $(\hat{\tau}_1^{(s)}, \dots, \hat{\tau}_K^{(s)}) \in [-1, 1]$ , is chosen as the sample points, where  $\hat{\tau}_i^{(s)} = \frac{\tau_i^{(s)} + \tau_{i+1}^{(s)}}{2}$ . Then, the solution error of each segment can be calculated by

$$e_k^{(s)} = \left| \dot{X}^{(s)}(\hat{\tau}_k^{(s)}) - \frac{t_s - t_{s-1}}{2} f^{(s)}(X_k^{(s)}, U_k^{(s)}, \hat{\tau}_k^{(s)}) \right| \quad (28)$$

where each column of  $e_k^{(s)}$  denotes the solution error of corresponding state at the sample points. Let  $e_{\max}^{(s)}$  be the column of  $e_k^{(s)}$  that contains the largest element of  $e_k^{(s)}$ . If the largest element of  $e_k^{(s)}$  is greater than the preset tolerance  $\epsilon_d$ , then the calculation accuracy should be improved by either increasing the interpolation polynomial degree or further dividing the current segment.

*Remark 4:* According to (26), the dynamics constraint is discretized at the LGR points, the calculation errors at these points are equal to zero. Therefore, (28) is introduced to evaluate the solution accuracy. The first term  $\dot{X}^{(s)}(\hat{\tau}_k^{(s)})$  is the results by interpolating the LRG points, while the second term is the results by solving the system dynamics.

To determine which way should be applied, the states curvature in segment  $s$  is first calculated by

$$\nu^{(s)}(\tau) = \frac{|\ddot{X}_m^{(s)}(\tau)|}{\left[1 + \dot{X}_m^{(s)}(\tau)^2\right]^{3/2}} \quad (29)$$

where  $X_m^{(s)}(\tau)$  is the state corresponding to the maximum component of  $e_{\max}^{(s)}$ . Let  $r_s = \nu_{\max}^{(s)}/\bar{\nu}^{(s)}$ , where  $\nu_{\max}^{(s)}$  and  $\bar{\nu}^{(s)}$  are the maximum and mean value of  $\nu^{(s)}(\tau)$ . Define the curvature tolerance  $r_{\max}$ , if  $r_s > r_{\max}$ , then we think there is a point, at which the curvature is significantly larger than that at other points of the current segment and the segment should be divided into more segments. If  $r_s \leq r_{\max}$ , then the curvature at this segment

has a uniform behavior and the calculation accuracy is improved by increasing the order of the polynomial.

In the case of  $r_s > r_{\max}$ , the number of subdivisions is calculated by

$$n_s = \lambda_1 \text{ceil} \left( \log_{10} \left( e_{\max}^{(s)} \right) - \log_{10}(\epsilon_d) \right) \quad (30)$$

where  $\lambda_1 > 0$  is a user-defined constant,  $\text{ceil}$  is the operator that rounds up to the next integer. To determine the location of the division, define the distribution function

$$F(\tau) = \int_{-1}^{\tau} \rho(\zeta) d\zeta \quad (31)$$

where  $\rho(\tau) = c\nu(\tau)^{1/3}$ ,  $F(+1) = 1$ . Then, the subdivision location satisfies  $F(\tau_i) - F(\tau_{i-1}) = 1/n_s$ .

In the case of  $r_s \leq r_{\max}$ , the solution accuracy is improved by increasing the collocation points, the number of updated LGR points is calculated by

$$N_s^* = N_s + \lambda_2 \text{ceil} \left( \log_{10} \left( e_{\max}^{(s)} \right) - \log_{10}(\epsilon_d) \right) \quad (32)$$

where  $\lambda_2 > 0$  is a user-defined parameter to regulate the growth of the segment.

*Remark 5:* The parameter  $r_{\max}$  can be treated as a tuning parameter that weights it should be a local or a global strategy to improve the solution accuracy. If  $r_s \leq r_{\max}$ , the solution is considered relatively smooth and a larger-degree polynomial is permitted. On the other hand, the solution is non-smooth if  $r_s > r_{\max}$ , a large-degree polynomial will seriously reduce the calculation efficiency and the current segment should be further divided. The adaptive law (30) and (32) consider the difference between the maximum solution error and the preset tolerance. The greater the maximum error is, the more the nodes or the segments are needed. The parameter  $\lambda_1$  or  $\lambda_2$  can regulate the growth of the points or the segments. If the value of  $\lambda_1$  or  $\lambda_2$  is great, the solution will converge to the permitted accuracy within a fewer iteration, but the number of nodes or segments are quite different in two adjacent iterations. If  $\lambda_1$  or  $\lambda_2$  is small, the number of nodes or the segments will grow slowly, while it may need more iterations to satisfy the permitted accuracy.

## IV. EXPERIMENTAL RESULTS

### A. Numerical Trajectory Planning

In this subsection, the A-RPM is applied for trajectories planning of a two link planar FFSM shown in Fig. 1. As shown in the first plot, the ground micro-gravity platform is composed of the motion capture system, a two-link FFSM system, and the air-bearing floor. The motion capture system is used to track the position and attitude of the manipulator system. The air-bearing floor is usually a marble floor used to create a very flat surface. The second plot illustrates the designed FFSM system, including a two link manipulator, a simulator of the spacecraft, and an industrial computer for control and data analysis. To simulate the behavior of an FFSM in the micro-gravity environment, the simulator and each joint of the manipulator are supported by air-bearings (see the third plot of Fig. 1), which work by creating a thin film of pressurized gas between the air-bearing floor and

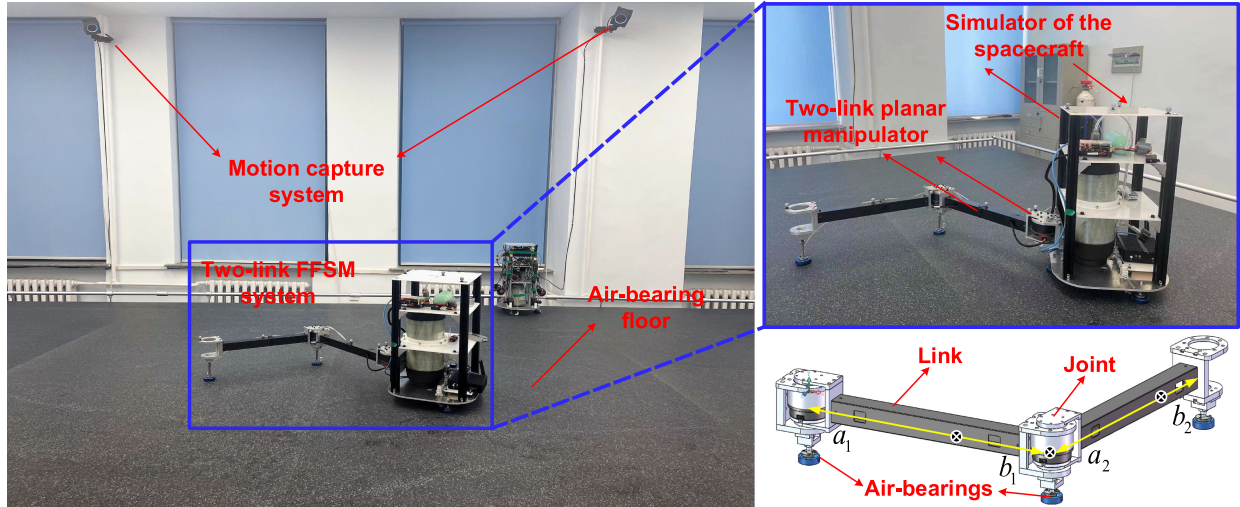


Fig. 1. Ground micro-gravity experimental platform of the FFSM system.

TABLE I  
SYSTEM PARAMETERS OF THE TWO-LINK PLANAR FFSM

Body No.	$m_i$ (kg)	$I_i$ (kg · m <sup>2</sup> )	$a_i$ (m)	$b_i$ (m)
0	15.20	0.1454	0.142	0.156
1	1.70	0.0590	0.364	0.142
2	1.20	0.0486	0.35	0.156

the system. This thin film compensates for the system's gravity and eliminates the friction between the floor and the system.

The parameters of this experiment system are given in Table I. The optimal problem is solved by using the GPOPS and SNOPT toolbox. In the platform, the spacecraft and the joints can only rotate along  $z$ -axis and move in a plane. The initial configurations of the spacecraft and the manipulator are set as  $\theta_b(t_0) = 0$ ,  $\dot{\theta}_b(t_0) = 0$ , and  $\theta_m(t_0) = [0, 0]^T$ ,  $\dot{\theta}_m(t_0) = [0, 0]^T$ , respectively. The desired configuration is  $\theta_m(t_f) = [\frac{\pi}{6}, \frac{\pi}{3}]^T$ ,  $\dot{\theta}_m(t_f) = [0, 0]^T$ ,  $\theta_b(t_f) \in [-\frac{\pi}{12}, \frac{\pi}{12}]$ ,  $\dot{\theta}_b(t_f) = 0$ . Considering the joint limitation in practical systems, the state constraints is chosen as  $\theta_{m1}, \theta_{m2} \in [-\frac{\pi}{2}, \frac{\pi}{2}]$ ,  $\dot{\theta}_{m1}, \dot{\theta}_{m2} \in [-0.9, 0.9]$ ,  $\theta_b \in [-\frac{\pi}{12}, \frac{\pi}{12}]$ ,  $\dot{\theta}_b \in [-0.6, 0.6]$ . The control inputs are limited by  $u_1 \in [-5, 5]^T$ ,  $u_2 \in [-4, 4]^T$ , and the final time  $t_f = 20$  s. The time interval  $[t_0, t_f]$  is initially divided into 10 segments, with 5 initial LGR points in each segment. The maximum iteration is 6, and the maximum number of LGR points in each segment is 20. The specific form of the cost functional is chosen as  $J = \|\theta_b(t_f)\|^2 + \|x_b(t_f) - x_b(t_0)\|^2 + \|y_b(t_f) - y_b(t_0)\|^2 + \int_{t_0}^{t_f} 0.6\|\dot{\theta}_b(t)\|^2 + 0.2\|\dot{\theta}_m(t)\|^2 dt$ . The tolerance is  $\epsilon_d = 1 \times 10^{-5}$ . The results are depicted in Figs. 2–3.

Fig. 2 shows the optimized base and joint trajectories. Fig. 2(a) plots the base attitude and the joint angles. The maximum offset of the base attitude is reduced to around 0.35 deg. Compared with variations of the joints, the base offset can be ignored, implying that if the joints rotate along the planned trajectories, the base motion has little influence on the motion of the entire system. The final attitude is included in the cost functional, so it can be observed that  $\theta_b$  decreases after a large deviation from its initial value. Fig. 2(b) presents the angular velocities of the base and joints. For reducing the base motion, the joints

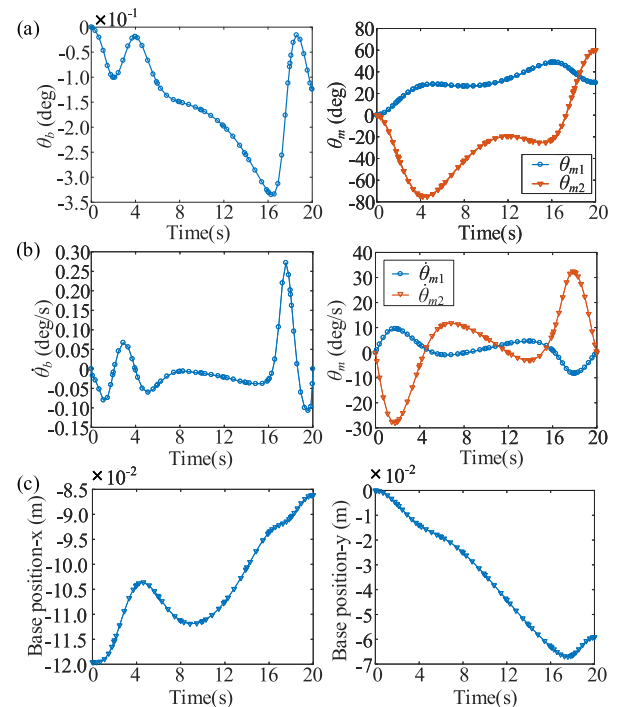


Fig. 2. Optimized trajectories of the base and the joints. (a) Base attitude and joints angles. (b) Angular velocities of the base and the joints. (c) Base displacement.

do not rotate directly to the preset values. Instead, they first rotate in the opposite direction and then rotate to the preset values. It can be also observed that the stability of the spacecraft sacrifices the response speed. However, this is acceptable for space manipulators, because it usually has long and more flexible arms, leading to their slow operation speed. Fig. 2(c) presents the base translation, the maximum displacement is 8.5 cm in the  $x$ -direction and 7.0 cm in the  $y$ -direction.

Fig. 3 shows the solution error of system states in each segment. In the first iteration, the maximum solution error is around  $5.297 \times 10^{-4}$  at  $t = 17$  s, which is greater than the preset tolerance. Therefore, the LGR points are reassigned in



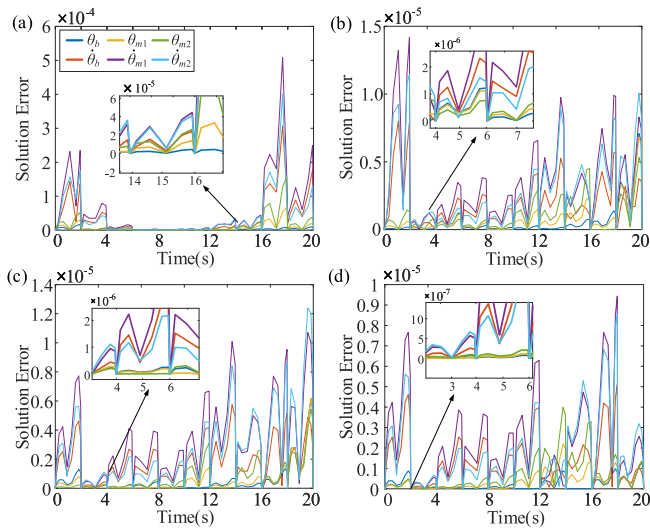


Fig. 3. Solution error of system states during iterations. (a) The first iteration. (b) The second iteration. (c) The third iteration. (d) The fourth iteration.

TABLE II  
COMPARISON OF THE A-RPM AND THE TRADITIONAL RPM

Tolerance	Method	Points	CPU Time /s	Error / $10^{-5}$
$10^{-3}$	RPM	35	6.9184	44.523
	A-RPM	50	6.2382	50.848
$10^{-4}$	RPM	40	16.2167	5.3082
	A-RPM	56	6.4106	7.7247
$10^{-5}$	RPM	57	36.5233	0.6078
	A-RPM	67	7.6697	0.9436

the following iterations until the error meets the requirement. In the fourth iteration, the solution errors of all states are within the preset tolerance, with the maximum error being  $0.9436 \times 10^{-5}$ . The calculation efficiency of the A-RPM and traditional RPM is given in Table II and the two methods are performed on the same computer. It can be observed that the two methods have almost the same CPU time when the preset tolerance is relatively great. However, with the improvement of the accuracy requirement, the CPU time of traditional RPM increases obviously, while that of the A-RPM remains almost unchanged.

### B. Experiment Analysis

This subsection verifies the proposed method on the micro-gravity ground FFMSM platform. For comparison, both the optimized trajectories shown in Fig. 2 and the trajectories under the minimum acceleration trajectory planning method (MATPM) are given to the system. The minimum acceleration in the MATPM refers to as the maximum acceleration of the trajectory is the smallest. The experiment results are presented in Figs. 4–6.

Figs. 4–5 show the system motion sequences under both methods. Obviously, the position and attitude of the spacecraft are influenced by the joint rotation in both cases. However, the variation of the spacecraft in A-RPM is smaller compared to that in MATPM, implying that the disturbance on the spacecraft is reduced when the joints move along the optimized trajectories.

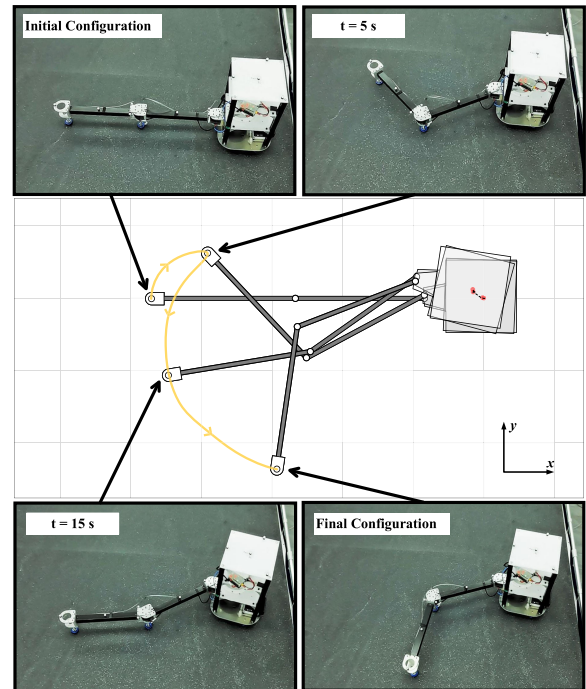


Fig. 4. System motion sequence under the A-RPM.

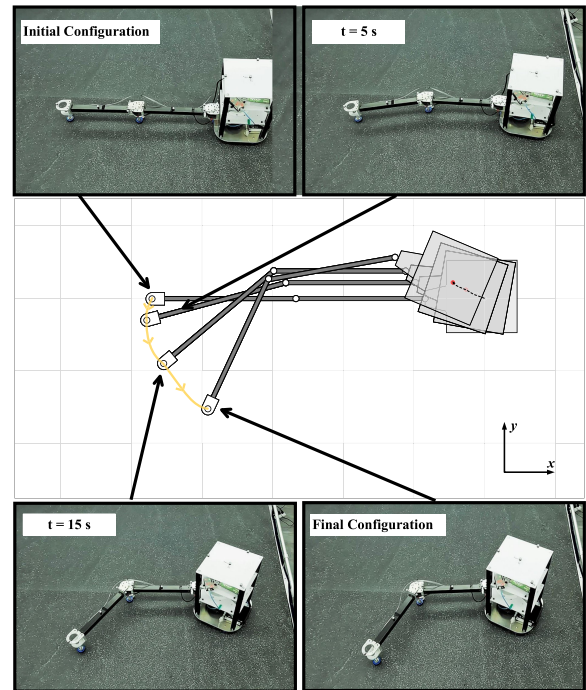


Fig. 5. System motion sequence under the MATPM.

The joints in the MATPM directly rotate to the preset values, while in the A-RPM they first rotate in the opposite direction ( $t = 5$  s) and then turn to the desired position to compensate for the impact on the spacecraft. The variation curves of system states are presented in Fig. 6. The final displacement of the spacecraft under A-RPM is 3.2 cm in the  $x$ -direction and 4.2 cm in the  $y$  direction, while the values respectively increase to

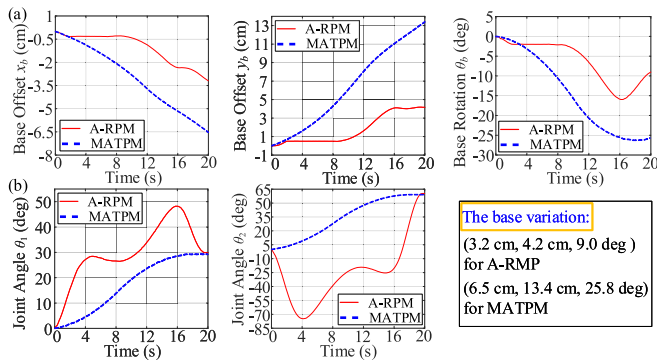


Fig. 6. Variation of system states. (a) Position and attitude of the spacecraft. (b) Joint angles.

6.5 cm and 13.4 cm under the MATPM. The proposed method reduces the planar movement by more than half. In terms of the base rotation, the maximum base rotation is 16.4 deg by A-RPM, but the final base rotation is reduced to 9.0 deg, which is consistent with the simulation results. In the MATPM, the base angle keeps getting bigger with the maximum value being 25.8 deg. Although the spacecraft in the experiment still has an undesired offset under the proposed method, the motion is dramatically reduced compared with MATPM.

In general, even though the base still moves when the joints rotate along the optimized trajectories, the range of the motion is greatly reduced. The experimental results and the simulation results show a similar trend but not exactly the same, which is due to the incomplete simulation of the ground micro-gravity platform to the space environment. Even so, the results still verify the advantage of the proposed method in reducing the base movement.

## V. CONCLUSION

For space manipulators working in free-floating mode, it is usually desired to maintain a stable but not precise base attitude in the navigation, communication, and precapture phase. This letter proposes an optimal control method to reduce the spacecraft variation generated by the joints' rotation. To obtain the numerical solution of the established optimization problem with satisfactory efficiency, the A-RPM is applied to discretize the continuous optimal control problem and transform it into an NLP. Experiments were conducted on a ground micro-gravity platform, which proved that the base variation can be dramatically reduced when the joints rotate along the optimized trajectories. Future work will focus on the task space trajectory planning and more accurate experiment verification.

## REFERENCES

- [1] R. Lampariello, H. Mishra, N. Oumer, P. Schmidt, M. D. Stefano, and A. Albu-Schäffer, "Tracking control for the grasping of a tumbling satellite with a free-floating robot," *IEEE Robot. Automat. Lett.*, vol. 3, no. 4, pp. 3638–3645, Oct. 2018, doi: [10.1109/LRA.2018.2855799](https://doi.org/10.1109/LRA.2018.2855799).
- [2] E. Papadopoulos and S. Dubowsky, "On the nature of control algorithms for free-floating space manipulators," *IEEE Trans. Robot. Automat.*, vol. 7, no. 6, pp. 750–758, Dec. 1991, doi: [10.1109/70.105384](https://doi.org/10.1109/70.105384).
- [3] G. Misra and X. Bai, "Optimal path planning for free-flying space manipulators via sequential convex programming," *J. Guid., Control, Dyn.*, vol. 40, no. 11, pp. 3019–3026, Nov. 2017, doi: [10.2514/1.G002487](https://doi.org/10.2514/1.G002487).
- [4] X. Lu and Y. Jia, "Trajectory planning of free-floating space manipulators with spacecraft attitude stabilization and manipulability optimization," *IEEE Trans. Syst., Man, Cybern. Syst.*, vol. 51, no. 12, pp. 7346–7362, Dec. 2021, doi: [10.1109/TSMC.2020.2966859](https://doi.org/10.1109/TSMC.2020.2966859).
- [5] F. James, S. V. Shah, A. K. Singh, K. M. Krishna, and A. K. Misra, "Reactionless maneuvering of a space robot in precapture phase," *J. Guid., Control, Dyn.*, vol. 39, no. 10, pp. 2419–2425, Oct. 2016, doi: [10.2514/1.G001828](https://doi.org/10.2514/1.G001828).
- [6] A. V. Rao, "A survey of numerical methods for optimal control," *Adv. Astronaut. Sci.*, vol. 135, no. 1, pp. 497–528, 2009.
- [7] V. H. Schulz, *Reduced SQP Methods for Large Scale Optimal Control Problems in DAE With Application to Path Planning Problems for Satellite Mounted Robots*. Ph.D. thesis, Univ. Heidelberg, Heidelberg, Germany, 1996.
- [8] D. N. Nenchev, K. Yoshida, P. Vichitkulsawat, and M. Uchiyama, "Reaction null-space control of flexible structure mounted manipulator systems," *IEEE Trans. Robot. Automat.*, vol. 15, no. 6, pp. 1011–1023, Dec. 1999, doi: [10.1109/70.817666](https://doi.org/10.1109/70.817666).
- [9] D. Garg, M. Patterson, W. W. Hager, A. V. Rao, D. A. Benson, and G. T. Huntington, "A unified framework for the numerical solution of optimal control problems using pseudospectral methods," *Automatica*, vol. 46, no. 11, pp. 1843–1851, Nov. 2010, doi: [10.1016/j.automatica.2010.06.048](https://doi.org/10.1016/j.automatica.2010.06.048).
- [10] D. Garg, W. W. Hager, and A. V. Rao, "Pseudospectral methods for solving infinite-horizon optimal control problems," *Automatica*, vol. 47, no. 4, pp. 829–837, Apr. 2011, doi: [10.1016/j.automatica.2011.01.085](https://doi.org/10.1016/j.automatica.2011.01.085).
- [11] F. Aghili, "A prediction and motion-planning scheme for visually guided robotic capturing of free-floating tumbling objects with uncertain dynamics," *IEEE Trans. Robot.*, vol. 28, no. 3, pp. 634–649, Jun. 2012.
- [12] X. Shao, G. Sun, C. Xue, and X. Li, "Nonsingular terminal sliding mode control for free-floating space manipulator with disturbance," *Acta Astronautica*, vol. 181, pp. 396–404, Apr. 2021, doi: [10.1016/j.actaastro.2021.01.038](https://doi.org/10.1016/j.actaastro.2021.01.038).
- [13] Y. Umetani and K. Yoshida, "Resolved motion rate control of space manipulators with generalized jacobian matrix," *IEEE Trans. Robot. Automat.*, vol. 5, no. 3, pp. 303–314, Jun. 1989, doi: [10.1109/70.34766](https://doi.org/10.1109/70.34766).
- [14] A. Izadbakhsh and P. Kheirkhan, "Nonlinear PID control of electrical flexible joint robots-theory and experimental verification," in *Proc. IEEE Int. Conf. Ind. Technol.*, Feb. 2018, pp. 250–255, doi: [10.1109/ICIT.2018.8352185](https://doi.org/10.1109/ICIT.2018.8352185).